Deformation-Induced Martensitic Characteristics in 304 and 316 Stainless Steels during Room-Temperature Rolling

VIJAY SHRINIVAS, S.K. VARMA, and L.E. MURR

The effect of grain size on the deformation-induced martensite (α') in 304 and 316 stainless steels (SS) during room-temperature rolling has been studied. Samples of four grain sizes of 52, 180, 229, and 285 μm in 304 and three grain sizes of 77, 125, and 200 μm in 316 SS have been rolled from 16 to 63 pct reduction in thicknesses to characterize the microstructures during the rolling deformation. The amount of α' formed increases with increase in the amount of deformation in both SS for a given grain size. The volume fraction of martensite formed increases with a decrease in grain size in 304 SS, while the α' martensite formation has been found to be grain size insensitive in 316 SS. The volume fraction of α' formed in 304 SS is always higher than that in 316 SS for a fixed percent reduction in thickness and grain size. This is attributed to the higher number of shear band intersections observed in 304 SS, which are considered to be the nucleation sites for the α' embryos. The lath martensite obtained at small true rolling strains changes to blocky type at higher true strains. The morphology of α' formed has been discussed and its characteristics obtained from rolling deformation have been compared with those earlier reported from the room-temperature tensile deformation.

I. INTRODUCTION

THE transformation from austenite to martensite in ferrous systems can be accomplished either by heat treatment or deformation of austenite. Two different types of martensites can be obtained by these methods. The heat treatment produces body-centered tetragonal (bct) martensite, while deformation can result in a martensite that can have either body-centered cubic (bcc) or hexagonal close-packed (hcp) crystal structures, known as α' and ε martensites, respectively.

The deformation-induced martensite may be classified under two categories: stress assisted or strain induced. Maxwell *et al.*[1] have indicated that the stress-assisted martensite is formed during the deformation when the stress levels simply provide for the reduction in driving force required for the transformation from austenite to martensite. The type of martensite formed by stress-assisted deformation involves the spontaneous nucleation and growth of martensite in a plate form,[1-5] usually in a manner similar to that obtained by thermal quenching of austenite. However, strain-induced martensite is a direct consequence of the plastic deformation and can be morphologically different from stress-assisted or thermally produced martensites. The production of lath-type martensite by strain-induced process appears to be quite common in ferrous systems. The literature also presents a point of view that the formation of ε martensite could be a prerequisite to α' formation. However, the formation of α' has been quite conclusively shown to be independent of ε martensite by several authors.[6,7] This article deals with mainly lath-type martensite, and thus, the following discussion will be confined to lath or α' martensite only.

The strain-induced martensite (α') forms by the plastic deformation of the parent austenite, where the proper defect structure is created and acts as an embryo for the transformation product. The potential nucleation sites for these embryos may include deformation twins, stacking faults, and the hcp martensites.[1,5,8] The appearance of an hcp structure in the transformation from austenite to martensite of Fe-Ni-Cr alloys was reported by Breedis and Robertson,[9] Binder,[10] Otte,[11] and Cina.[12] Kelley and Nutting[13] and Bilby and Christian[14] have surmised that the hcp phase may be associated with stacking faults in the parent austenite and that these stacking faults may be the nucleation sites for the martensitic transformation. Venables[15] conducted a study on a thin film of deformed 18-8 stainless steels (SS) and inferred that a possible sequence in the transformation could be from fcc(γ) to hcp(ε) and finally to bcc(α') crystal structures. Bastien and Dedieu[16] studied the austenite to martensite transformation in low-carbon 18-8 SS and noted that while simple cooling of the steel to very low temperatures produces very little α', the plastic deformation at temperatures slightly higher or lower than room temperature produces a considerable amount of α'. Lagneborg[17] concluded that the martensite produced during the deformation of 18-8 steels at room temperature occurred in the shape of thin needles in contact with a (111) habit plane and that the intersection between the ε sheets constituted a preferred nucleation site for martensite.

Lecroisey and Pineau[5] and Venables[15] established that the shear band intersections could be very effective sites for strain-induced martensite nucleation in 304 SS. Olsen and Cohen[18-21] and Olsen and Azrin[22] did the pioneering work in this field of deformation-induced martensite. They developed a model for estimating the volume fraction of martensite formed considering the course of shear band formation, their intersections, and the probability

VIJAY SHRINIVAS, Graduate Student, S.K. VARMA, Professor, and L.E. MURR, Chairman and Mr. and Mrs. Macintosh Murchison Professor, are with the Department of Metallurgical and Materials Engineering, The University of Texas at El Paso, El Paso, TX 79968-0520.

Manuscript submitted June 13, 1994.

of an intersection generating a martensitic embryo. They reported that the transformation curve has a sigmoidal shape, which reaches a saturation at fractions below 100 pct.

Hecker *et al.*[23] have studied the effect of different strain states (uniaxial and biaxial) and strain rates on α' formation in 304 SS. They observed that at low strains, α' formed more readily at high strain rates (10^3/s) than at low strain rates (10^{-3}/s). However, at true strains higher than 0.25, they noted that the situation was just the reverse and attributed this phenomenon to adiabatic heating, which inhibits α' formation at high strain rates. Murr *et al.*[24] have observed the regular (lath) morphology for low strains and blocky morphology at high strains as a result of coalescence of α' embryos. Lecroisey and Pineau[5] have noted the morphology of α' as being only lath type. They did not observe any plate-type martensite even at low temperatures. Brooks *et al.*[7] have conducted an *in situ* study on the formation of α' in three different SS, 16 pct Cr-14 pct Ni, 16 pct Cr-12 pct Ni, and 18 pct Cr-10 pct Ni, and proposed that the martensite always nucleates from suitable dislocation configurations, which are generated by the stress associated with the transformation, and the presence of pre-existing embryos is not required for martensitic nucleation as the heterogeneities can be provided by dislocations formed prior to the transformation.

Bogers and Burgers[25] were among the first to illustrate the mechanism of bcc α' nucleation from fcc austenite. They proposed that the production of specific defect arrays on {111} planes and their intersection produces a stable bcc volume element through two invariant plane strains. They also proposed that specific arrays can be created randomly within the microshear band intersections by systematic stacking of faults, which provide specific partial displacements on each {111} plane. The first invariant plane strain involves displacement on every $(\bar{1}11)$ plane for the specific orientation of 1/3 of the twinning shear $a/6[\bar{1}1\bar{2}]$. The second invariant plane strain involves displacements of every $(1\bar{1}1)$ plane of $a/16[1\bar{1}\bar{2}]$ or 3/8 of the twinning shear $a/6[1\bar{1}\bar{2}]$. In addition to these shears, the transformation involves a dilational component. In forming the α' martensite nucleus, the shape change is that of partial dislocations and the final nucleus will involve more complex lattice invariant deformations to produce invariant plane surfaces which are semicoherent between the bcc volume and the fcc matrix.[24]

Murr *et al.*[24] have also explained the growth phenomenon of α' embryos. They proposed from their transmission electron microscopy (TEM) observations that at low strain levels for a particular stress state, the α' formation is restricted to small intersection volumes, and with increasing strain, the α' product appeared to grow. In uniaxial tension tests, the growth looked similar to long laths, and in the case of biaxial tension, it was an irregular and blocky α' product. They concluded from these observations that α' laths grow by the formation of many embryos at intersections spaced closely along a shear band. They have also observed the evidence of α' martensite growing out of (111), planes, some in specific crystallographic directions and others at random. They believe that the regular, blocky polyhedra were being formed by the coalescence of individual embryos.

Varma *et al.*[26] have recently studied the effect of grain size on the α' formation in 304 and 316 SS during tensile testing and rolling at room temperature. It was found that the amount of α' formed in 304 SS increased with the increase in true strains for both modes of deformation, but considerably larger amounts were formed in rolling compared to those formed in tension for similar true strains. It has also been shown that α' formation is grain size dependent in 304 SS. The α' formation was also observed in 316 SS in rolling, but it was not detected during the tensile deformation. The grain size dependence on α' formation was also confirmed in 316 SS during rolling. It must, however, be noted that a larger volume fraction of α' formed in 304 SS during rolling than in 316 SS for similar true rolling strains.

The purpose of this article is to report the microstructural evolution during the room-temperature rolling process in 304 and 316 SS. The characteristics of α' formation in these two SS will be compared with those found in tensile testing in an earlier study.[26] The effect of grain size on the development of microstructures in terms of potential nucleation sites during the deformation has been explored.

II. EXPERIMENTAL DETAILS

The chemical compositions of the 304 and 316 SS used in this study are shown in Table I. This table indicates that nickel content of 13.48 pct (all compositions are in weight percent) is present in 316 SS, while 304 SS contains only 8.19 pct. Also the molybdenum contents in 304 and 316 SS are 0.27 and 2.34 pct, respectively. Besides these two elements, the compositions of the two SS can be considered to be similar.

The 304 SS samples were subjected to an isochronal annealing for 1 hour at 1100 °C, 1200 °C, and 1300 °C to obtain grain sizes of 180, 229, and 285 μm, respectively. The isothermal annealing of 316 SS at 1175 °C for 1 and 3 hours results in grain sizes of 125 and 200 μm, respectively. The as-received 304 and 316 SS were both in the annealed condition with grain sizes of 52 and 77 μm, respectively. The as-received and annealed samples were subjected to rolling on a STANAT-1101 machine to achieve 16, 32, 43, 55, and 66 pct reductions in thickness. The strain rates were assumed to be essentially constant in all the cases.

The martensite (α') obtained from plastically deformed austenite (γ) is ferromagnetic and is readily detected by magnetic measurements. The magnetic

Table I. Chemical Compositions of 304 and 316 SS (in Weight Percent)

Steel	C	Mn	P	S	Si	Ni	Cr	Mo	Co	Cu
304	0.054	1.730	0.034	0.014	0.350	8.190	18.33	0.270	0.120	0.120
316	0.057	1.860	0.024	0.019	0.580	13.48	17.25	2.340	0.020	0.100

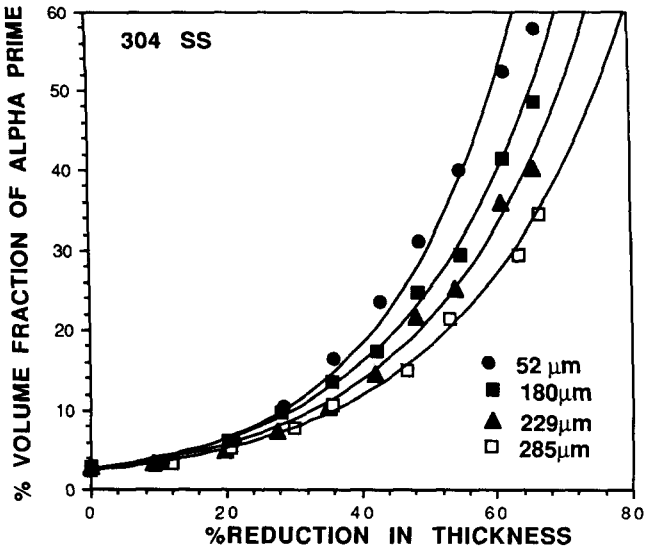

Fig. 1 — Variation in the percent volume fraction of α' martensite as a function of percent reduction in thickness during room-temperature rolling in 304 SS for four different grain sizes of 52, 180, 229, and 285 μm.

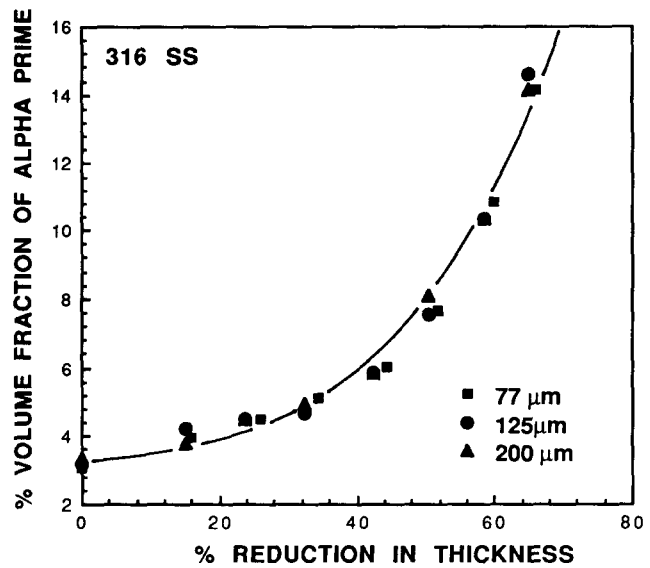

Fig. 2 — Variation in the percent volume fraction of α' martensite as a function of percent reduction in thickness during room-temperature rolling in 316 SS for three different grain sizes of 77, 125, and 200 μm.

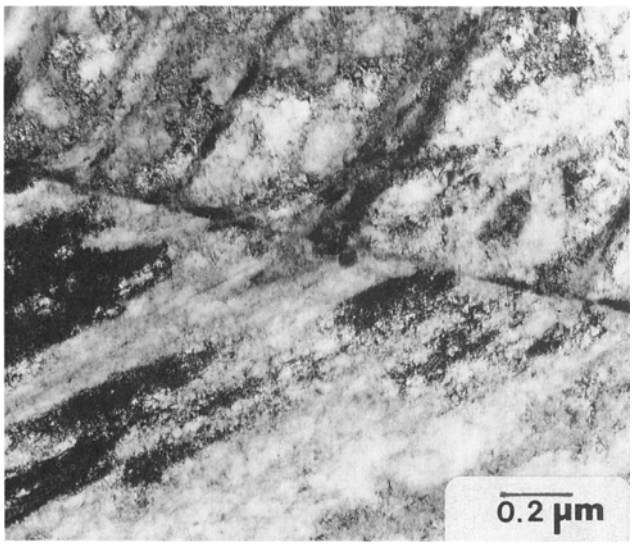

Fig. 3 — Grain-boundary nucleation of α' martensite in 316 SS during room-temperature rolling.

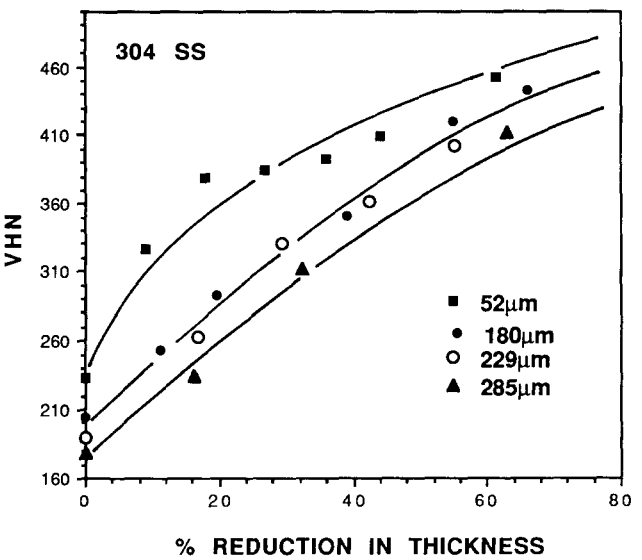

Fig. 4 — Variation in the microhardness values as a function of percent reduction in thickness during room-temperature rolling in 304 SS for four different grain sizes of 52, 180, 229, and 280 μm. Note that the data points for the grain sizes of 180 and 229 μm have been fitted with a single curve.

permeability of a sample can be measured with the help of a ferritescope. This is a two-point probe which, when placed on a sample, is energized by the low-frequency magnetic field and induces a voltage. This voltage induced is a direct measure of the magnetic permeability. The ferritescope usually gives the ferrite number of the specimen, which is converted into a volume fraction of martensite with the help of a standard calibration curve. The magnetic measurements were obtained on as annealed, ground, and deformed samples. Microhardness testing was done on the samples with a surface finish corresponding to final mirror polish, obtained by 0.03 μm alumina powder on the polishing wheels, using a SHIMADZU-3931 hardness tester.

Transverse wafers of 0.8 to 1.0-mm thickness were cut from the center of the deformed samples. The wafers were cut by a Buehler Isomet cutting machine with a diamond or alumina blade using Buehler Isomet fluid as a lubricant. The wafers were then hand ground (both sides) on grit papers 320 through 600 up to a thickness of 0.15 to 0.2 mm. The discs of 3-mm diameter were punched out from the ground wafer and were ready for jet polishing. Struer's Tenupol-3 equipment was used for jet polishing. The electrolyte used was 95 pct methanol and 5 pct perchloric acid by volume. The solution was cooled to −20 °C, and the following parameters were used to

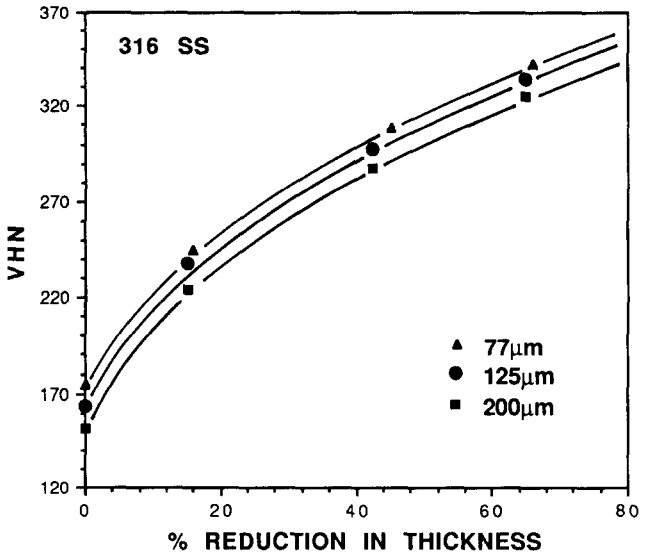

Fig. 5—Variation in the microhardness values as a function of percent reduction in thickness during room-temperature rolling in 316 SS for three different grain sizes of 77, 125, and 200 μm.

polish the samples: voltage = 30 V; sensitivity = 8; and flow rate = 1.5. The polished samples were rinsed in acetone, methanol, and absolute ethanol, in this order. A Hitachi H-8000 scanning transmission electron microscope (STEM) was used at 200 kV to observe the microstructures. A minimum of three foils were observed for a given condition, and the entire sample was scanned for features such as shear bands, their intersections, twin faults, and martensite. Dark-field images were obtained by using the selected area diffraction (SAD) method.

III. RESULTS AND DISCUSSION

A. *Volume Fraction of α' and Microhardness Values vs Percent Reduction in Thickness during Room-Temperature Rolling*

Figure 1 shows the variation in the volume fraction of α' martensite with reduction in thickness for four different grain sizes: 52, 180, 229, and 285 μm, in 304 SS. It has been observed that the amount of α' increases with an increase in percent reduction in thickness for all four grain sizes. It appears that the increase in the amount of α' formed per unit percent reduction in thickness increases at a faster rate after about 20 pct. Even though the data in this figure have been fitted with a continuous curve, it must be noted that an S-shaped curve could as well be obtained by the interpolation of the experimental points for each grain size. Obviously, for certain grain sizes, the saturation exhibited by typical S-shaped curves has not reached. The S-shaped curves were speculated by Olsen and Cohen[18–21] and Olsen and Azrin,[22] as noted earlier in this article.

Figure 2 shows the variation in volume fraction of α' martensite with percent reduction in thickness for three different grain sizes: 77, 125, and 200 μm, in 316 SS. The behavior shown by 316 SS appears to be similar to 304 SS. It must be noted that the formation of α' in 316 SS has not been reported in the open literature. It

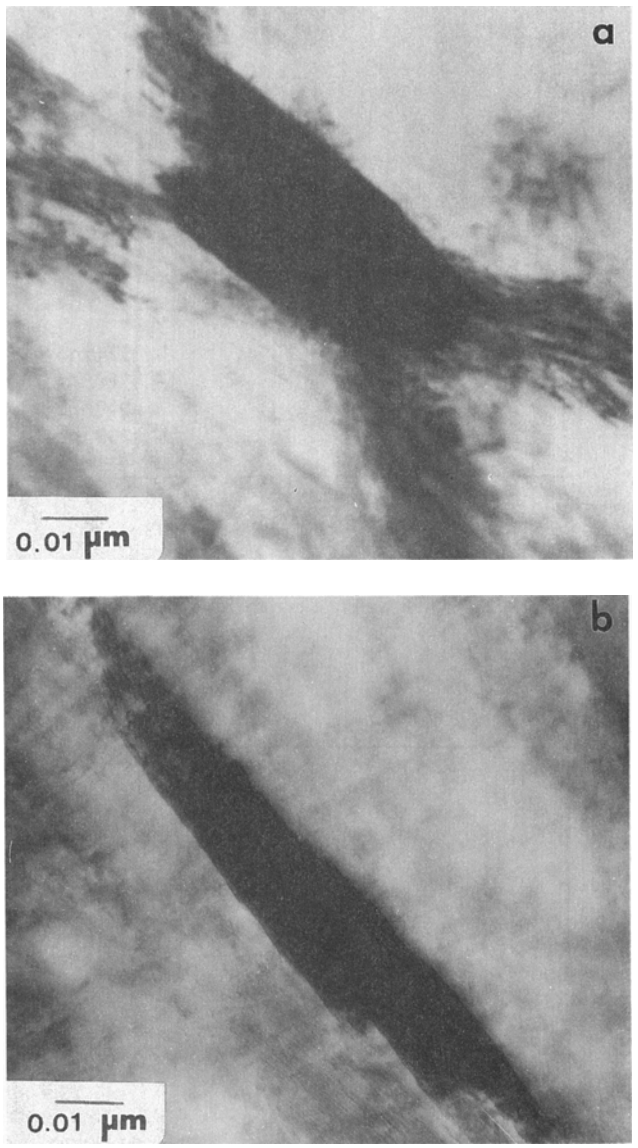

Fig. 6—Morphology of deformation-induced martensite in 304 SS with grain sizes of (*a*) 52 μm and (*b*) 229 μm.

can be seen from Figure 2 that the α' formation in 316 SS is insensitive to the changes in grain sizes, at least for the grain size range from 77 to 200 μm used in this study. Figure 1, however, shows that the amount of α' increases with a decrease in grain size for the range of percent reduction in thickness from nearly 20 to 66. Thus, we clearly see that the α' does form in both steels, but they are not both grain size sensitive. This should rule out the possibility of a grain-boundary nucleation site for 316 SS, but α' has been found to form at the grain boundaries in 316 SS in this research, as shown in Figure 3. However, the possibility of grain boundaries as the intersection sites for the shear bands, together with grain boundaries as the place where martensite growth may terminate, across the grains in question should not be ruled out.

We feel that the role of grain boundaries in the formation of deformation-induced martensite may be explained on the basis of the stacking fault energy (SFE)

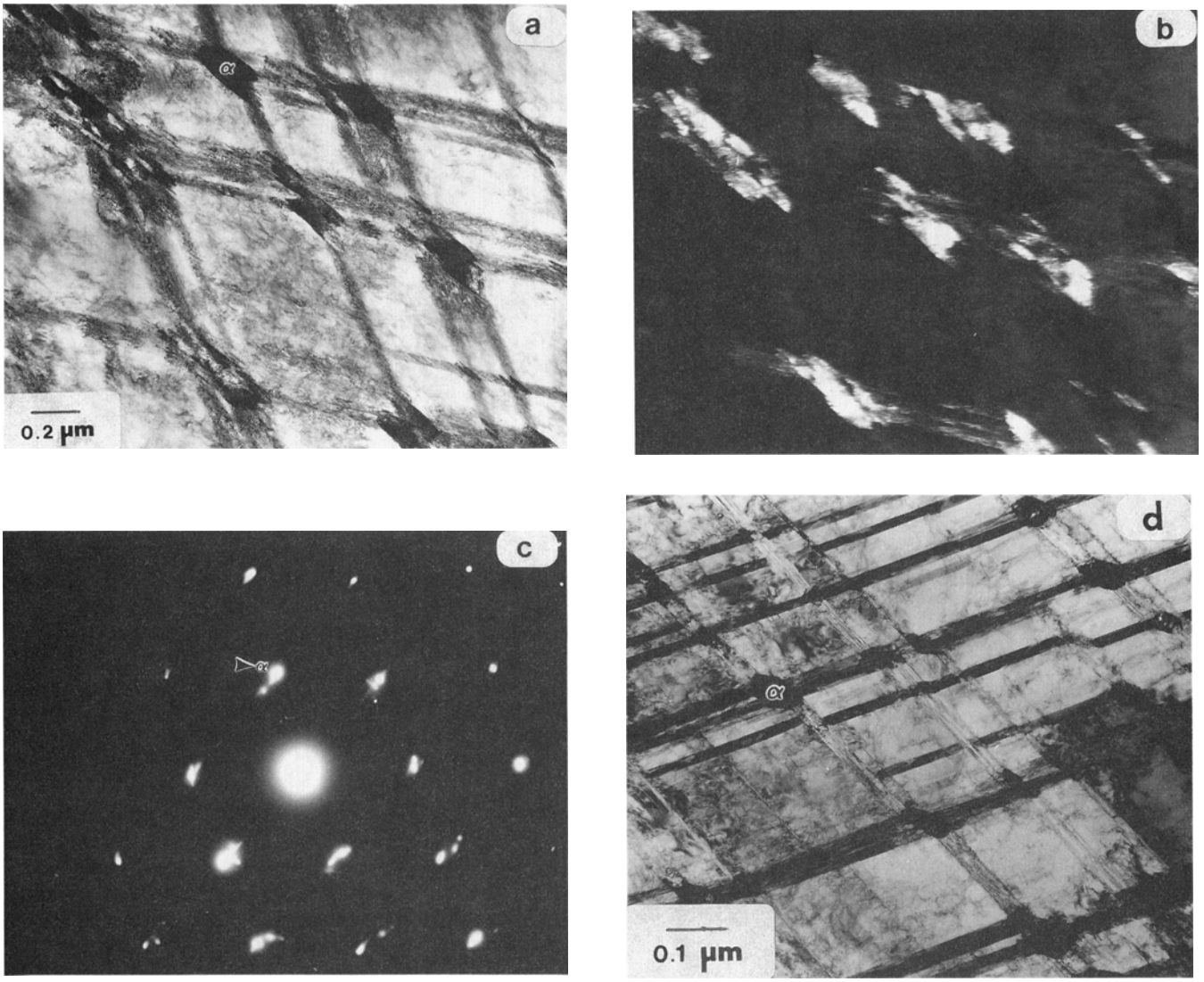

Fig. 7—The (*a*) origin-field image, (*b*) dark-field image, and (*c*) diffraction pattern from the area shown in (a) for the 304 SS samples deformed to a strain of 16 pct. The arrow in (c) indicates the diffraction spot used to get the dark-field image shown in (b). (*d*) Low-magnification view of an area similar to that shown in (a).

value of 316 SS (40 mJ/m^2)[27] relative to 304 SS (21 mJ/m^2).[28,29] The lower SFE value for 304 SS will obviously result in more planar slip compared to the easier cross slip, which is to be expected in 316 SS. This would indicate a larger number of shear band intersections in 304 SS on the basis of per unit area for smaller grain sizes. However, it could also mean grain size independent nucleation in 316 SS during the deformation process especially at higher strain values.

Figures 4 and 5 show the variation in the microhardness values as a function of percent reduction in thickness during rolling for 304 and 316 SS, respectively. Figure 4 shows the changes in the hardness values at different percent reduction in thicknesses; however, note that single curve fitting has been applied for the data points of 180 and 229 μm grain sizes since the two grain sizes are quite similar, while the differences in the amount of α' formed increase with a decrease in grain size at various percent reduction in thicknesses in 304 SS, as shown in Figure 1. Thus, it can be concluded that the contribution of α' martensite to the hardness values has to be insignificant compared to the main grain size strengthening shown by 304 SS in Figure 4. This fact becomes more convincing in the case of 316 SS, where Figure 2 shows similar amounts of α' martensite for different grain sizes while Figure 5 indicates basically grain size strengthening differences only. Thus, we find that α' apparently is not a very effective strengthener.

B. *Morphology of α' Martensite in 304 and 316 SS of This Study*

Typical morphology of an α' martensite in both 304 and 316 SS observed in this study is shown in Figure 6. The morphology is of lath type, as the substructure predominantly consists of dense dislocations and there is no evidence of twins in them. The sharp boundaries along the length of the laths appear to be coherent. In certain cases, ledges (Figure 6(b)), which are indications of semicoherent boundaries, have also been observed.

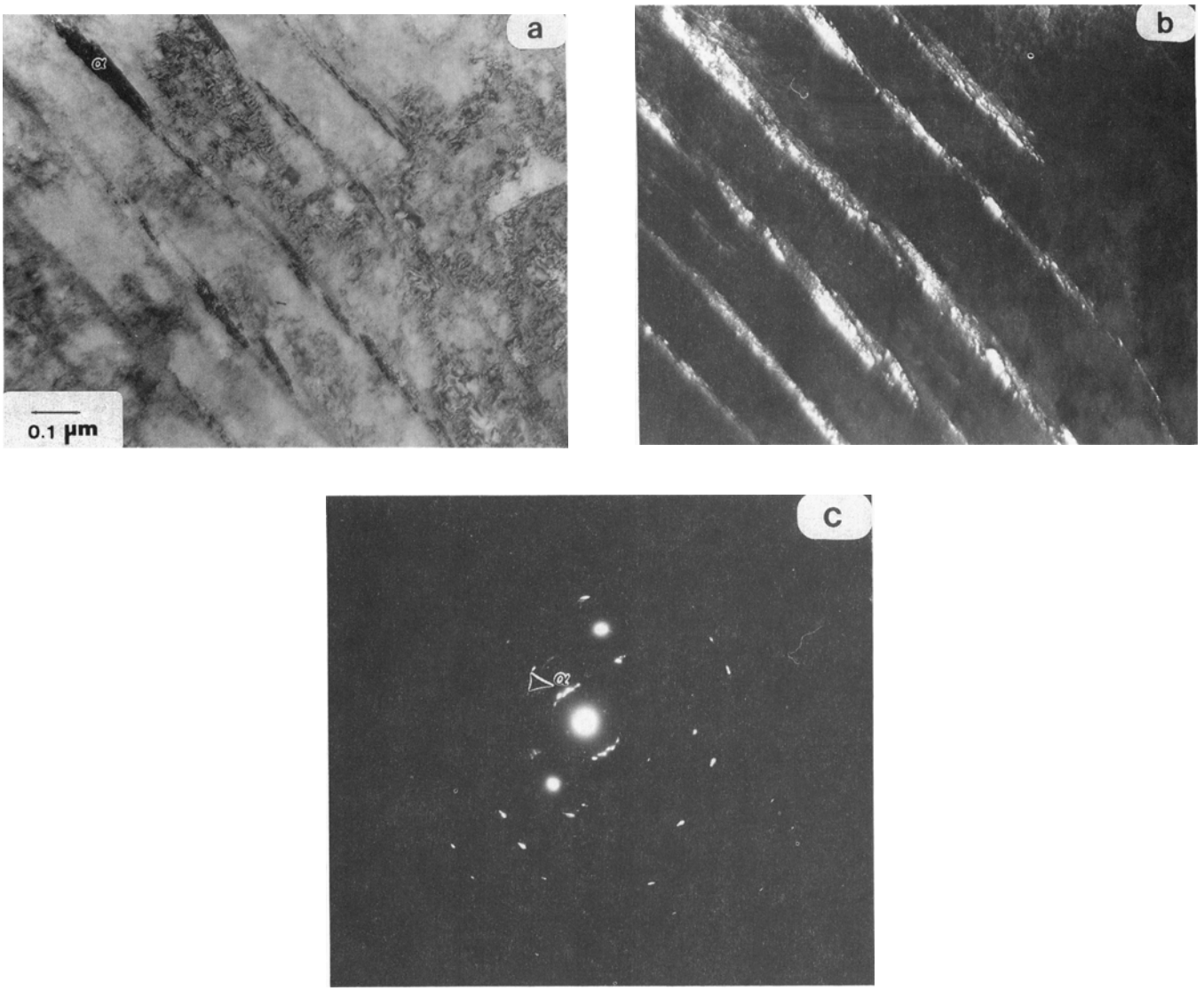

Fig. 8—The (*a*) bright-field image, (*b*) dark-field image, and (*c*) diffraction pattern from the area shown in (a) for the 304 SS samples deformed to a strain of 32 pct. The arrow in (c) indicates the diffraction spot used to get the dark-field image shown in (b).

However, this appearance could be due to irregular etching of the ends or edges that coincide with the surfaces of the film. The diffused edges seen on the shorter end of the laths appear to be incoherent.

C. *Microstructural Evolution during Room-Temperature Rolling of 304 SS*

The only microstructural feature observed in the as-annealed condition was the presence of grain boundaries with complete absence of any substructure within the grains. Figure 7 shows the microstructure for 304 SS samples deformed to a strain of 16 pct. The figure clearly shows the presence of shear bands, their intersections, and α' nucleation at the shear band intersections. The presence of α' has been confirmed with dark-field imaging shown in Figure 7(b), which comes from the spot marked on the SAD pattern in Figure 7(c). It has been observed that not all shear band intersections result in the nucleation sites for α' formation, as shown in Figure 7(d) (which is a micrograph showing a similar area as in Figure 7(a) but taken at a lower magnification). This is because α' nucleation depends not only on the probabilities of shear band intersection and the intersections resulting in an α' embryo but also on a critical nucleation size and on satisfying the requisite strain-invariant conditions to form martensite.[23,24]

Figure 8 shows the microstructure developed after the 304 SS samples have been deformed to a strain of 32 pct during room-temperature rolling. The growth of α' in comparison to the sizes observed at 16 pct strain, shown in Figure 7(a), is quite obvious. The shear band intersections cannot be observed in this micrograph, as the specimen stage is tilted slightly to obtain better contrast between α' and the parent austenite phase. The growth of martensite can be attributed to the increase in α' nucleating centers and their coalescence caused by the increased strain.[6,7,23,24] The dark-field image corresponding to the diffraction spot indicated in Figure 7(c) clearly shows the increase in α' after 32 pct deformation compared to the case of 16 pct deformation shown in Figure 7(b).

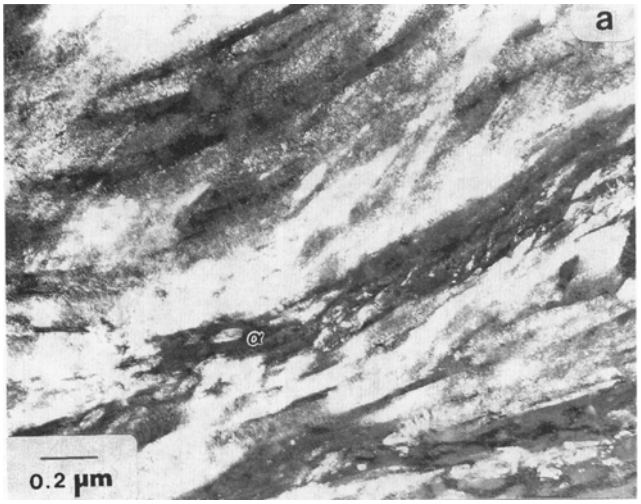

Fig. 9—The (*a*) bright-field image and (*b*) diffraction pattern from the area shown in (a) for the 304 SS samples deformed to a strain of 63 pct.

The shear bands and α' martensite are quite difficult to resolve in the microstructure when the 304 SS samples are rolled to 63 pct reduction in their thicknesses, as shown in Figure 9. The presence of martensite can only be confirmed by the SAD patterns. The SAD pattern from these samples, Figure 9(b), shows the presence of parent austenite and α' martensite. The change in morphology from lath to, perhaps, blocky martensite with increase in strain has also been reported by Murr *et al.*[24] for the case of 304 SS deformed in biaxial tension.

We can summarize the main features of microstructural developments during room-temperature rolling of 304 SS as follows: (a) deformation of grains occurs by shear band formations; (b) the number of nonparallel shear bands increases with increase in strain; (c) some of the shear band intersections become the nucleating site for the α' martensite formation; (d) the growth of α' martensite occurs due to the increase in number of shear band intersections as a result of increase in strain; and (e) there is a change in the morphology of α' from lath to blocky martensite and a loss of resolution for both shear bands and α' martensite at higher strains. We do not know the reasons for the change in morphology observed in this study and the results reported by other researchers[24] in this field. However, it may be speculated that the interface becomes unstable after the lath martensite develops a critical dimension, which may result in the development of blocky martensite.

D. *Microstructural Evolution during Room-Temperature Rolling of 316 SS*

The as-annealed samples of 316 SS indicate the presence of only grain boundaries with relatively clean grain interiors. On increasing the deformation to 16 pct strain, the microstructure is found to consist of shear bands, as shown in Figure 10(a). However, the shear band intersections were rarely observed at this strain. No α' nucleation was observed, which was consistent with the ferritescope data, which showed little or no change in ferrite readings. The dark-field image (Figure 10(b)) of the bright-field image shown in Figure 10(a) shows the substructure within the band, which is slightly difficult to resolve, and the presence of ε martensite, if any, is inconclusive from the diffraction pattern.

An example of the microstructures obtained in the samples deformed to 43 pct strain is shown in Figure 11. Contrary to an earlier hypothesis that α' may not form in 316 SS, α' nucleation was observed at this strain. Once again, as in 304 SS of Figure 8, typical shear band intersections and α' are not seen due to the slight tilting of the sample stage to obtain better contrast between α' martensite and the parent austenite. The presence of α' martensite has been confirmed by both dark-field imaging and SAD patterns, as shown in Figures 11(b) and (c), respectively.

At still higher strain, namely, 65 pct, shear bands and α' become extremely difficult to resolve (Figure 12), as was observed in the case of 304 SS. The similarities in the morphological changes from lath to blocky martensite between 304 and 316 SS at this high strain must be noted. Once again, the SAD pattern (Figure 12(b)) shows the presence of α' martensite unambiguously.

E. *Comparison of Microstructural Developments between 304 and 316 SS*

The 316 SS, though being austenitic like 304 SS, tends to behave differently during rolling from the microstructural point of view in two different ways. (a) It is considerably less rolling sensitive to α' formation compared to 304 SS. To illustrate this, a deformation of 16 to 18 pct in 304 SS results in the α' nucleation, while only shear band formation could be observed at this strain in 316 SS. Also, the volume fraction of α' formed in 304 SS, particularly at high strains, is considerably higher than that in 316 SS for comparable grain sizes. (b) The 316 SS is grain size insensitive to α' formation as opposed to the definite grain size sensitivity exhibited by 304 SS, as discussed earlier.

F. *Stress State Dependence on α' Formation in 304 and 316 SS*

Varma *et al.*[26] have reported that α' was formed, as detected by the ferritescope, in 304 SS having grain sizes

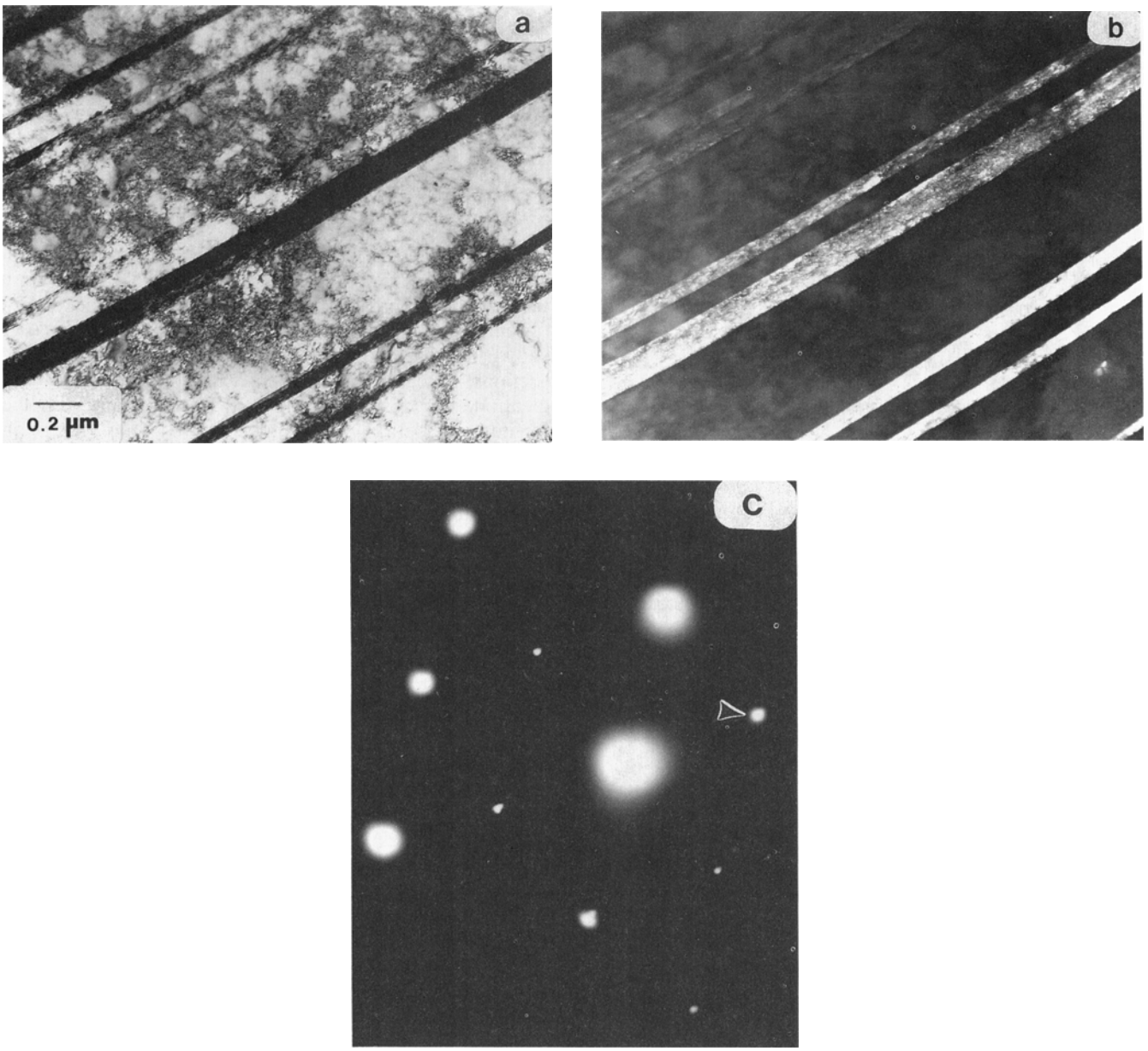

Fig. 10—The (*a*) bright-field image, (*b*) dark-field image, and (*c*) diffraction pattern from the area shown in (a) for the 316 SS samples deformed to a strain of 16 pct. The arrow in (c) indicates the diffraction spot used to get the dark-field image shown in (b).

of 52, 180, and 285 μm during room-temperature tensile testing. On changing the stress state from uniaxial tension to multiaxial rolling, it has been observed in this study that 304 SS of similar grain sizes formed much higher volume fraction of α' martensite than during tensile testing for similar strains. To illustrate this, let us consider the variations in the volume fraction of martensite with true strain for tensile (uniaxial) and rolling (multiaxial) deformation of 304 SS conforming to a grain size of 52 μm. It can be seen from Figure 13 that the difference in volume fractions of martensite between rolling and tensile deformation, $\delta\alpha'$ ($=\alpha'_{\text{rolling}} - \alpha'_{\text{tension}}$) is negligible at a true strain of 0.1 and increases to about 14 pct at 0.4 true strain for a grain size of 52 μm. Comparison beyond a true strain of 0.4 was not considered meaningful, as tensile testing was performed only up to this strain. The variations of $\delta\alpha'$ with true strains in rolling and tensile deformations for two grain sizes of 52 and 285 μm are shown in Figure 13. The different types of curves shown after curve fitting the data in the two graphs of this figure do not have any special significance except to show that the higher volume fraction of α' martensite is formed during rolling than in tensile deformation at both the highest and the lowest grain sizes of this study.

Varma *et al.*[26] also reported that no change in the volume fraction of α' martensite formed as a function of true strain in 316 SS during tensile deformation for different grain sizes. However, samples of similar grain sizes subjected to rolling in this study indicate significant amounts of α' formation. These observations are shown in Figure 14. In this case, it is not necessary to plot $\delta\alpha$

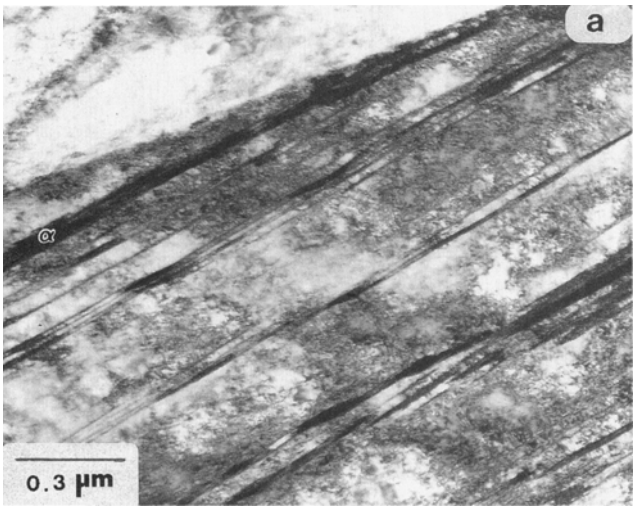

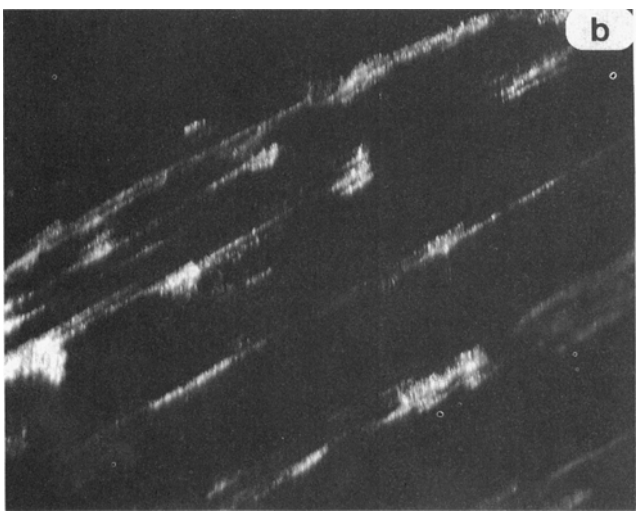

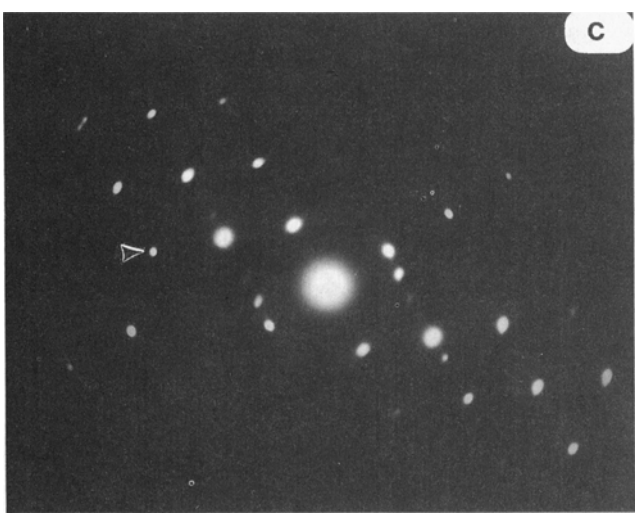

Fig. 11—The (*a*) bright-field image, (*b*) dark-field image, and (*c*) diffraction pattern from the area shown in (a) for the 316 SS samples deformed to a strain of 43 pct. The arrow in (c) indicates the diffraction spot used to get the dark-field image shown in (b).

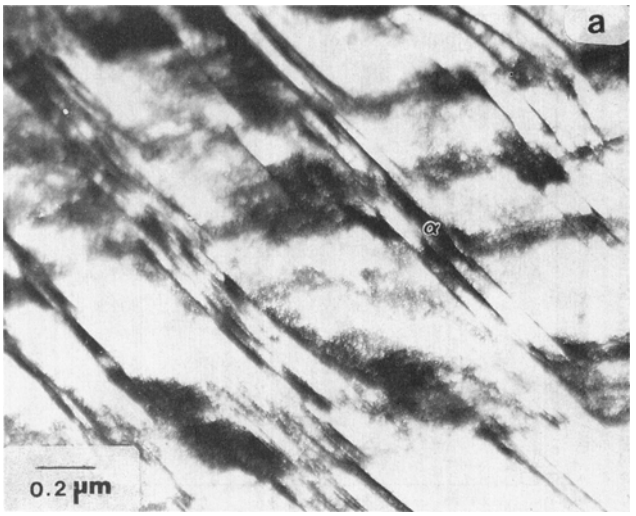

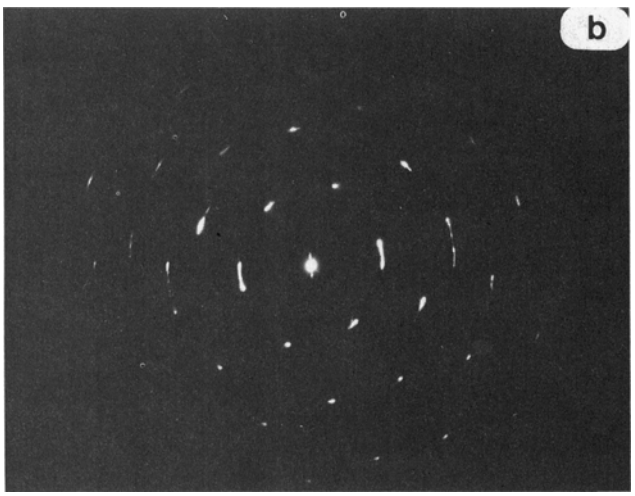

Fig. 12—The (*a*) bright-field image and (*b*) diffraction pattern from the area shown in (a) for the 316 SS samples deformed to a strain of 65 pct.

vs true strain, as the α' curve is a flat line, and the $\delta\alpha'$ *vs* true strain curve would be the same as α' *vs* true strain for rolling.

Staudhammer *et al.*[30] proposed from the TEM work on the samples of 304 SS deformed in the uniaxial and biaxial (tensile) modes that multiple slip systems get activated in biaxial mode and this results in a large number of shear band intersections, which can provide an extra incremental fraction of nucleation sites for α' formation compared to those in the uniaxial mode for similar true strain values. It is believed that the increase in both the number of shear band intersections and probability of α' nucleation as stress state is altered in the present case, *i.e.*, from uniaxial to multiaxial, manifested in the form of more extensive multiple slip, is responsible for the higher volume fraction of α' formation during rolling of 304 and 316 SS compared to that in tension.

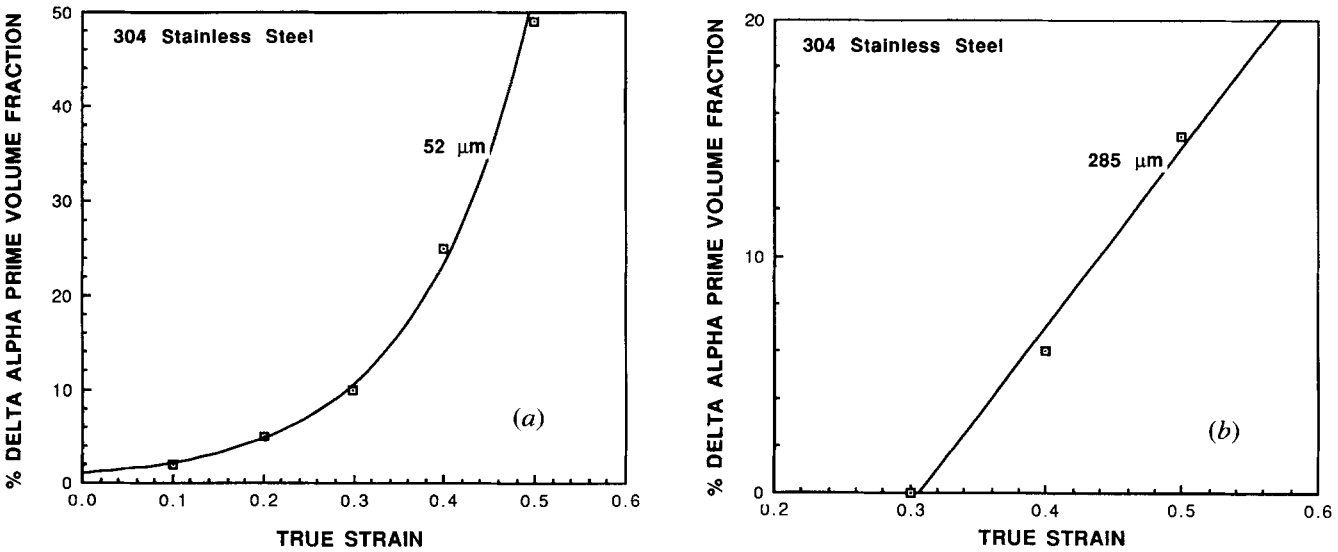

Fig. 13—The effect of strain state on α' formation in 304 SS. Variation in the percent $\delta\alpha'$ ($=\alpha'_{rolling} - \alpha'_{tension}$) with true strain in rolling and tensile deformations for grain sizes of (*a*) 52 μm and (*b*) 285 μm.

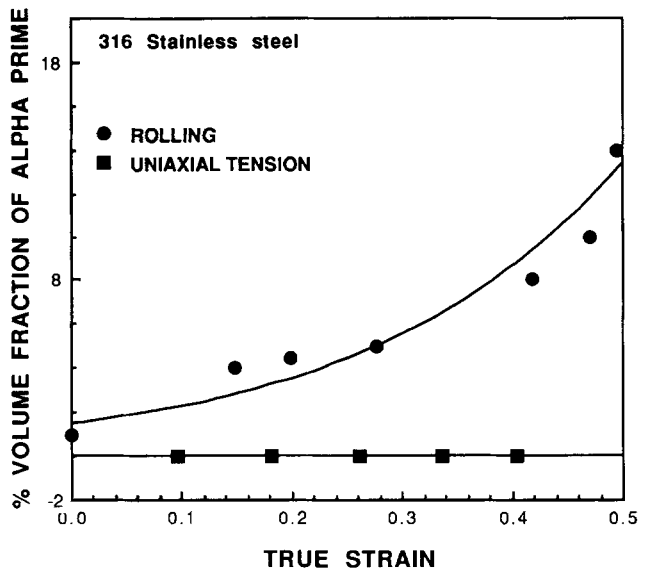

Fig. 14—The effect of strain state on α' formation in 316 SS. Variation in the percent volume fraction of α' martensite as a function of true strain in rolling and uniaxial tension for a grain size of 77 μm.[126]

IV. CONCLUSIONS

1. The volume fraction of α' martensite formed with an increase in true rolling strains has the following characteristics: (a) it increases for both 304 and 316 SS; (b) it is grain size sensitive in 304 SS and increases with a decrease in grain size; and (c) it is grain size insensitive in 316 SS.
2. The microhardness values as a function of true rolling strain indicate that the formation of α' martensite during rolling is not a very effective strengthener compared to its counterpart thermal martensite found in other ferrous systems.
3. The lath-type morphology of α' martensite has been found in both SS at low true rolling strain values, while the blocky-type morphology appears to be formed at higher strains.
4. The formation of α' martensite was found to be delayed to higher true strains in 316 SS due to, perhaps, higher SFE compared to 304 SS. The number of shear band intersections, which have been found to be the main nucleation site for α' formation, is dependent on the SFE value.
5. The amount of α' martensite formed in 304 SS has been found to be always higher than that formed in 316 SS for similar grain sizes and true rolling strains.
6. The volume fraction of α' martensite is also stress state dependent. The uniaxial tension produces less α' compared to the multiaxial state during rolling under similar experimental conditions due to the multiple slip system being activated in multiaxial systems.

ACKNOWLEDGMENTS

The authors would like to thank Dr. K.P. Staudhammer of Los Alamos National Laboratory for providing the ferritescope for this study. One of the authors (VS) acknowledges the financial support, in part, from a General Services Administration (GSA) grant (Number PF 90-018), which is administered by the Institute for Manufacturing and Materials Management at the University of Texas at El Paso (UTEP). Dr. C.S. Niou's help in the TEM sample preparation technique was very valuable in this research.

REFERENCES

1. P.G. Maxwell, A. Goldberg, and J.C. Shyne: *Metall. Trans.*, 1974, vol. 5, pp. 1305-18.
2. J.R. Patel and M. Cohen: *Acta Metall.*, 1953, vol. 1, pp. 531-38.
3. I. Tamura, T. Maki, and H. Hato: *Trans. Jpn. Iron Steel Inst.*, 1970, vol. 10, pp. 165-67.
4. T. Maki, S. Shimooka, M. Umemoto, and I. Tamura: *Trans. Jpn. Iron Steel Inst.*, 1972, vol. 13, pp. 400-03.

5. F. Lecroisey and A. Pineau: *Metall. Trans.*, 1972, vol. 3, pp. 387-96.
6. T. Suzuki, H. Kojima, K. Suzuki, T. Hashimoto, and M. Ichihara: *Acta Metall.*, 1977, vol. 27, pp. 1151-62.
7. J.W. Brooks, M.H. Loretto, and R.E. Smallman: *Acta Metall.*, 1979, vol. 27, pp. 1829-38.
8. P.L. Manganon and G. Thomas: *Metall. Trans.*, 1970, vol. 1, pp. 1577-94.
9. J.F. Breedis and W.D. Robertson: *Acta Metall.*, 1963, vol. 11, pp. 547-59.
10. W.O. Binder: *Met. Progr.*, 1950, vol. 58, pp. 201-07.
11. H. Otte: *Acta Metall.*, 1957, vol. 5, pp. 614-27.
12. B. Cina: *J. Iron Steel Inst.*, 1955, vol. 179, pp. 230-32.
13. P.M. Kelley and J. Nutting: *J. Iron Steel Inst.*, 1961, vol. 197, pp. 199-203.
14. B.A. Bilby and J.W. Christian: *J. Iron Steel Inst.*, 1961, vol. 197, pp. 122-27.
15. J.A. Venables: *Phil. Mag.*, 1962, vol. 7, pp. 35-44.
16. P.G. Bastien and J.M.B. Dedieu: *J. Iron Steel Inst.*, 1956, vol. 183, pp. 254-59.
17. R. Lagneborg: *Acta Metall.*, 1964, vol. 12, pp. 823-43.
18. G.B. Olsen and M. Cohen: *Metall. Trans. A*, 1975, vol. 6A, pp. 791-95.
19. G.B. Olsen and M. Cohen: *Metall. Trans. A*, 1976, vol. 7A, pp. 1897-1904.
20. G.B. Olsen and M. Cohen: *Metall. Trans. A*, 1976, vol. 7A, pp. 1905-14.
21. G.B. Olsen and M. Cohen: *Metall. Trans. A*, 1976, vol. 7A, pp. 1915-23.
22. G.B. Olsen and M. Azrin: *Metall. Trans. A*, 1978, vol. 9A, pp. 713-21.
23. S.S. Hecker, M.G. Stout, and K.P. Staudhammer: *Metall. Trans. A*, 1982, vol. 13A, pp. 619-26.
24. L.E. Murr, K.P. Staudhammer, and S.S. Hecker: *Metall. Trans. A*, 1982, vol. 13A, pp. 627-35.
25. A.J. Bogers and W.G. Burgers: *Acta Metall.*, 1964, vol. 12, pp. 255-61.
26. S.K. Varma, J. Kalyanam, L.E. Murr, and V. Srinivas: *J. Mater. Sci. Lett.*, 1994, vol. 13, pp. 107-11.
27. L.E. Murr: *Interfacial Phenomena in Metals and Alloys*, TechBooks, Herndon, VA, 1975, pp. 145-48.
28. M.J. Whelan, P.B. Hirsch, R.W. Horne, and W. Bollman: *Proc. R. Soc. A*, 1957, vol. 240, pp. 524-38.
29. L.E. Murr: *Thin Solid Films*, 1969, vol. 4, pp. 389-412.
30. K.P. Staudhammer, L.E. Murr, and S.S. Hecker: *Acta Metall.*, 1983, vol. 31, pp. 267-74.